Key Points:
- Ridging South Atlantic Anticyclones are accompanied by Rossby wave breaking (RWB) aloft in 44% of the cases
- Ridging highs that are accompanied by RWB lead to more precipitation over South Africa than those that are not
- Ridging highs bring more precipitation over the southern and less precipitation over the northeastern part of South Africa in the future

Correspondence to:
I. Ivanciu,
iivanciu@geomar.de

Author Contributions:
Conceptualization: Ioana Ivanciu, Thando Ndarana, Katja Matthes
Formal analysis: Ioana Ivanciu, Thando Ndarana, Katja Matthes
Methodology: Ioana Ivanciu, Thando Ndarana
Software: Ioana Ivanciu, Thando Ndarana, Sebastian Wahl
Visualization: Ioana Ivanciu
Writing – original draft: Ioana Ivanciu, Thando Ndarana, Katja Matthes, Sebastian Wahl

On the Ridging of the South Atlantic Anticyclone Over South Africa: The Impact of Rossby Wave Breaking and of Climate Change

Ioana Ivanciu[1] , **Thando Ndarana[2]** , **Katja Matthes[1]** , and **Sebastian Wahl[1]**

[1]GEOMAR Helmholtz Centre for Ocean Research Kiel, Kiel, Germany, [2]Department of Geography, Geoinformatics and Meteorology, University of Pretoria, Hartfield, South Africa

Abstract Ridging South Atlantic Anticyclones contribute an important amount of precipitation over South Africa. Here, we use a global coupled climate model and the ERA5 reanalysis to separate for the first time ridging highs (RHs) based on whether they occur together with Rossby wave breaking (RWB) or not. We show that the former type of RHs are associated with more precipitation than the latter type. The mean sea level pressure anomalies caused by the two types of RHs are characterized by distinct patterns, leading to differences in the flow of moisture-laden air onto land. We additionally find that RWB mediates the effect of climate change on RHs during the twenty-first century. Consequently, RHs occurring without RWB exhibit little change, while those occurring with RWB contribute more precipitation over the southern and less precipitation over the northeastern South Africa in the future.

Plain Language Summary The high pressure system located above the South Atlantic Ocean occasionally extends eastward over South Africa, leading to winds that blow onshore and carry moisture from the warm waters of the Southwest Indian Ocean to the coast. These events, termed ridging highs (RHs), bring an important contribution to precipitation over the southern and eastern parts of South Africa. Their occurrence is related to the propagation and breaking of atmospheric waves at the boundary between the troposphere and the stratosphere. This study categorizes RHs based on the behavior of atmospheric waves above and shows that events that are accompanied by wave breaking result in more precipitation over South Africa. In addition, model simulations are used to investigate the impact of climate change during the twenty-first century on RHs and the associated precipitation. Although the model predicts that in total South Africa will experience drier conditions in the future, RHs contribute to this drying trend only in the northeastern part of the country. In the southern part of South Africa, the model simulates that RHs will bring more precipitation in the future.

1. Introduction

Semi-arid South Africa receives most of its annual precipitation during the summer months over the eastern part of the country (Roffe et al., 2019). Winter rainfall occurs in the southwestern part of the country and the southeastern coast receives rainfall through the entire year (Engelbrecht et al., 2015; Roffe et al., 2019). These rainfall patterns are caused by mesoscale convective complexes (Blamey & Reason, 2012) and synoptic scale weather systems. The latter include the all-season cut-off low pressure systems (COLs) (Favre et al., 2013), tropical temperate troughs (TTTs; Harrison, 1984; Hart et al., 2012) and ridging South Atlantic Anticyclones, henceforth ridging highs (RHs). A RH occurs when the anticyclone extends east and wraps around the southern tip of Africa (Tyson & Preston-Whyte, 2000).

RHs are central to the moisture budget of South Africa because they are the main mechanism that facilitates the transport of moisture from the Southwest Indian Ocean (Dyson, 2015; Ndarana et al., 2021), and therefore critical to rainfall occurrence in the region. The Agulhas Current flows along the east coast of South Africa and is involved in complex interactions with the atmosphere (Jury & Goschen, 2020). Its warm waters result in high evaporation (Lee-Thorp et al., 1999; Rapolaki et al., 2020; Rouault et al., 2000) and provide an important source of moisture (Nkwinkwa Njouodo et al., 2018, 2021; Rouault et al., 2002; Singleton & Reason, 2006). Southerly and southeasterly onshore winds caused by RHs, advect the moisture and lead to precipitation on land (Blamey & Reason, 2009; Rapolaki et al., 2020). As a result, RHs contribute 60% of the summer rainfall days in the summer rainfall region (Ndarana et al., 2021) and 46% of the annual rainfall in the all-year rainfall region (Engelbrecht et al., 2015). COLs and TTTs, which co-occur with RHs, provide dynamical lifting mechanisms of moist air.

COLs contribute 25%–35% of the annual rainfall over the southern, eastern and central South Africa (Favre et al., 2013). At country scale, TTTs contribute 30% of the total monthly rainfall between October and March (Hart et al., 2013).

Several recent studies considered the upper level dynamics that might influence the initiation of the ridging process and found that they are associated with synoptic Rossby wave trains aloft (Ndarana et al., 2018, 2022). These Rossby waves may venture into non-linear regimes and break (McIntyre & Palmer, 1983), a process referred to as Rossby wave breaking (RWB). RWB can be viewed as a dissipating mechanism of wave packets (Wirth et al., 2018). Ndarana et al. (2018) showed that RHs may be associated with RWB in the upper troposphere and lower stratosphere, lasting for the entire evolution of the ridging process, and causing positive upper tropospheric potential vorticity (PV) anomalies that induce an anticyclonic circulation. These positive anomalies, in turn, extend to the surface to induce the ridging process (Ndarana et al., 2022). However, precisely what proportion of RWB events are associated with RHs and whether the behavior of the latter differs according to whether there is RWB aloft are still open questions. Further more, the influence of increasing concentrations of greenhouse gases (GHGs) in the twenty-first century on this relationship has not been explored yet. Thus, the questions we explore are.

1. What proportion of RHs are accompanied by RWB?
2. Do RHs occurring with RWB differ from those occurring without RWB in their evolution and in their effect on precipitation?
3. Will RHs and their impact on precipitation change in the twenty-first century in response to climate change?

The last question, investigated here for the first time, is of particular importance given that models predict a reduction in precipitation under climate change in the southern part of Africa (Almazroui et al., 2020; Dosio et al., 2019; Rojas et al., 2019) and considering the contribution of RHs to precipitation in this region.

2. Data and Methodology

We analyze RHs in the coupled climate model FOCI (Matthes et al., 2020) with a horizontal resolution of 1.8° and 95 vertical levels and in the ERA5 reanalysis (Hersbach et al., 2018, 2020) whose fields were interpolated to the model gird for an adequate comparison. FOCI distinguishes itself from other global coupled climate models through its capability to combine a module for simulating the ozone chemistry in the atmosphere, MOZART3 (Kinnison et al., 2007) with an ocean nest, INALT10X (Schwarzkopf et al., 2019), that enhances the ocean resolution around southern Africa to 0.1°. Therefore, the model resolves the mesoscale features of the Agulhas System and simulates an ozone field consistent with the atmospheric dynamics. The increased ocean resolution is important for the latent and sensible heat fluxes over the Agulhas Current (Rouault et al., 2003) and for precipitation (Singleton & Reason, 2006).

One historical and three twenty-first century ensembles are analyzed, each comprising three members. The historical ensemble is the same as the "REF" ensemble described by Ivanciu et al. (2021), which we analyze for the 1980–2009 period and we denote PAST. The first twenty-first century ensemble, FUTURE, represents continuations of the PAST simulations into the future under the high emission scenario SSP585, characterized by 1135 ppm CO_2 and an additional 8.5 W m^{-2} radiative forcing in 2100. The second ensemble, GHG, also follows SSP585, but ozone depleting substances are kept constant at their 1991–2000 climatological annual cycle, such that the ozone hole does not recover and only GHGs drive changes in this ensemble. In the third ensemble, OZONE, GHGs are instead kept constant at their 1991–2000 annual cycle, such that ozone recovery is the sole driver of changes. Here, we focus our analysis on the 2070–2099 period.

To validate our model results against observations, we employ the ERA5 mean sea level pressure (MSLP), temperature, horizontal winds and geopotential on pressure levels for the period 1980–2009 and the CPC Global Unified Gauge-Based Analysis of Daily Precipitation data provided by the NOAA PSL, Boulder, Colorado, USA, at 0.5° horizontal resolution (Chen et al., 2008).

RHs over South Africa are identified based on MSLP using the method of Ndarana et al. (2018). RWB events are identified following the algorithm of Ndarana and Waugh (2011), using PV between −2.5 and −1.5 PVU (1 PVU = $10^6 K m^2 s^{-1} kg^{-1}$) on isentropic surfaces. Then, for every ridging high, we test if it is accompanied by a RWB event by checking if RWB occurs in the domain 20°W–40°E and in the time interval from two days prior to
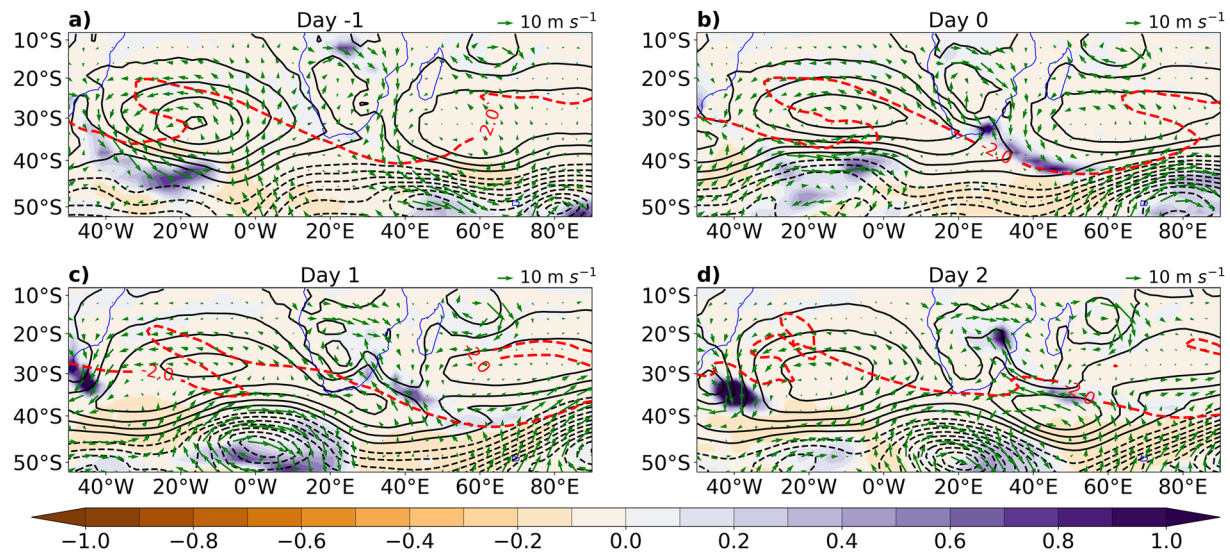
Figure 1. Example of ridging high (RH) accompanied by Rossby wave breaking (RWB) in FOCI: black contours depict the mean sea level pressure (MSLP), every 4 hPa, solid above 1010 hPa and dashed below, the color shading depicts precipitation anomalies (mm day^{-1}), the arrows depict the wind anomalies at 850 hPa (m s^{-1}) and the red dashed contour shows −2 PVU on the 350 K isentrop. The evolution of the event is shown from day −1 (a) to day +2 (d).

two days after the inception of ridging. A detailed description of the identification algorithms for RHs and RWB can be found in the Supporting Information S1.

3. Results and Discussion

A connection between RHs over South Africa and RWB aloft was reported by Ndarana et al. (2018) in reanalysis data. We first test if this relationship is captured by our coupled climate model. Figure 1 shows the evolution of a RH in the model, starting 1 day prior to the ridging. The South Atlantic Anticyclone extends progressively over South Africa until day 2, when a high pressure system breaks off from it and advances eastward over the Indian Ocean (black contours in Figure 1). This evolution is in good agreement with the RHs described by Ndarana et al. (2018). Simultaneously, the −2 PVU contour on the 350 K isentropic surface, depicted in red in Figure 1, is severely deformed throughout the evolution of the RH, signaling that RWB is taking place. This demonstrates that FOCI is capable of simulating RHs accompanied by RWB. Figure 1 also depicts how the RH brings onshore wind anomalies along the southern and eastern coasts of South Africa, transporting moisture on land and leading to positive precipitation anomalies that advance northward along the coast as the ridging progresses.

As Figure 1 depicts a single ridging event, the question of how often the RHs are accompanied by RWB arises. Out of 1872 (1969) RHs identified in FOCI (ERA5) over the period 1980–2009, 43% (44%) occurred together with RWB aloft and 57% (56%) occurred without RWB. These results are remarkably consistent between the model and the reanalysis. From a seasonal perspective, RHs with RWB dominate in summer and autumn, while RHs without RWB dominate in winter and spring (Figure S1 in Supporting Information S1). In total, we identified 534 RHs in summer, the season with the most events, comparable with the 699 summer events identified by Ndarana et al. (2021) over 39 years. Both of these numbers translate to 18 events in one summer. At the end of the twenty-first century, 38% and 62% of the 1936 RHs identified between 2070 and 2099 occur with and without RWB, respectively. The decrease in the proportion of RHs with RWB is consistent with the poleward shift in RWB that accompanies the poleward shift of the midlatitude jet under climate change in FOCI (Ivanciu et al., 2022), in agreement with Barnes and Hartmann (2012).

3.1. Characterization of Ridging Highs With and Without Rossby Wave Breaking

We now wish to understand the differences between RHs occurring with and without RWB in FOCI. To this end, we composite RHs with RWB and without RWB, separately, for the PAST ensemble and we show in Figures 2a–2d anomalies in MSLP and 200 hPa PV for days zero and one of each composite. Day zero represents
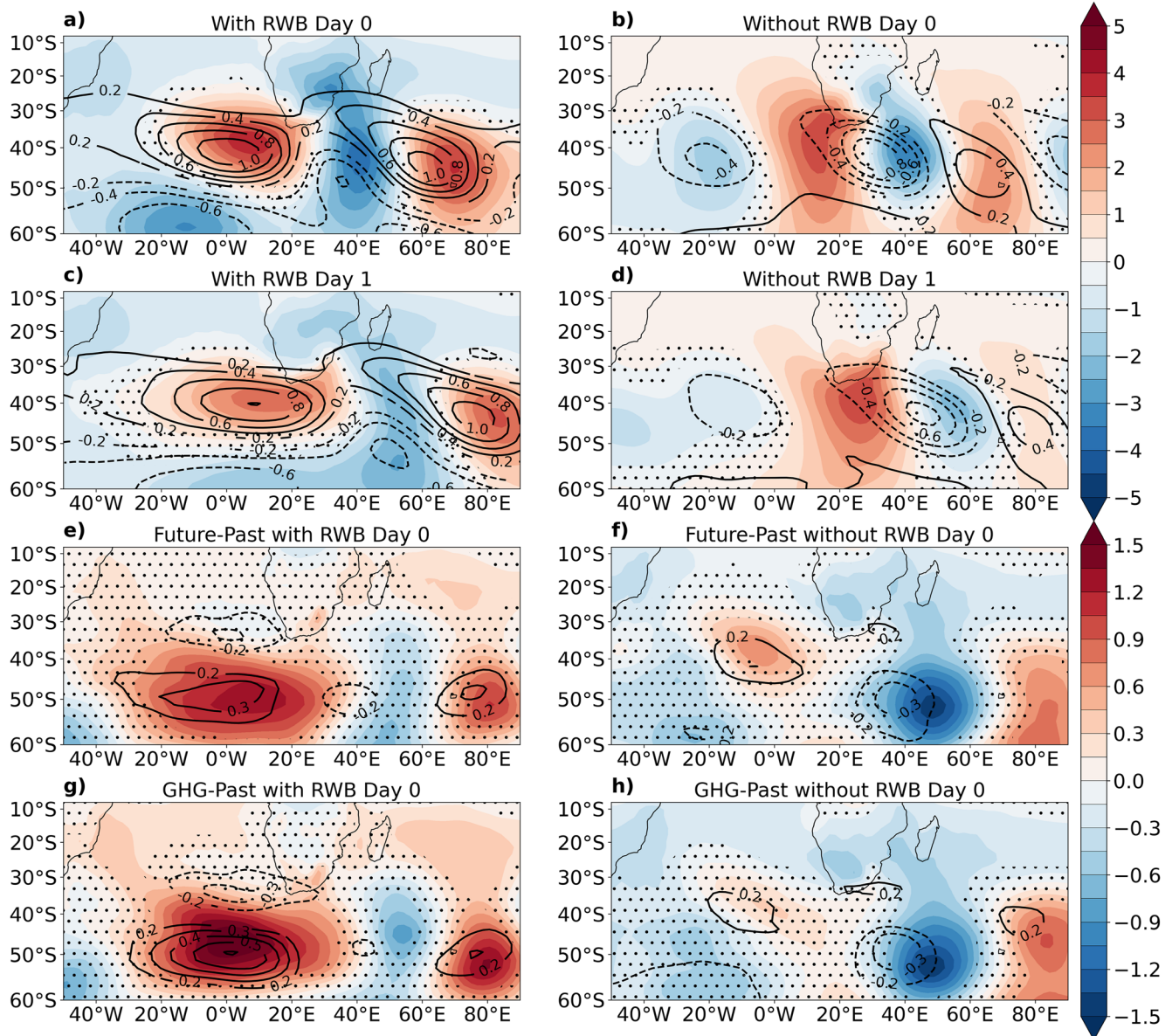
Figure 2. Composites of ridging highs (RHs) with (a, c) and without (b, d) Rossby wave breaking (RWB) at day 0 (a, b) and day 1 (c, d) of ridging for the period 1980–2009. Anomalies of mean sea level pressure (MSLP) (hPa) and of 200 hPa PV (PVU) are depicted by the color shading and by the contours, respectively. Total (e, f) and greenhouse gase (GHG)-induced (g, h) change, between 2070–2099 and 1980–2009, in the day 0 anomalies associated with RHs with (e, g) and without (f, h) RWB. The stippling masks anomalies that are not significant at the 95% confidence interval. Only significant PV anomalies are plotted.

the day when the South Atlantic Anticyclone first extends eastward of 25°E. Similar composites obtained for ERA5 are shown in Figure S2 in Supporting Information S1 and their patterns are in good agreement with the model, with small differences in magnitude present.

Both categories of RHs are characterized by positive MSLP anomalies in the Southeastern Atlantic Ocean, negative MSLP anomalies southeast of Africa, and positive MSLP anomalies farther east, that migrate eastward as the ridging progresses. There are however important differences in the shape and extent of these anomalies. In the case of RHs with RWB, the positive anomalies are elongated in the zonal direction, being flanked by negative anomalies south of 50°S. The positive anomalies occurring without RWB have a much larger meridional extent, reaching not only farther south, but also deeper inland. In fact, the entire South Africa is covered by positive MSLP anomalies at day 1, in contrast to the composites with RWB, where the positive anomalies are mostly
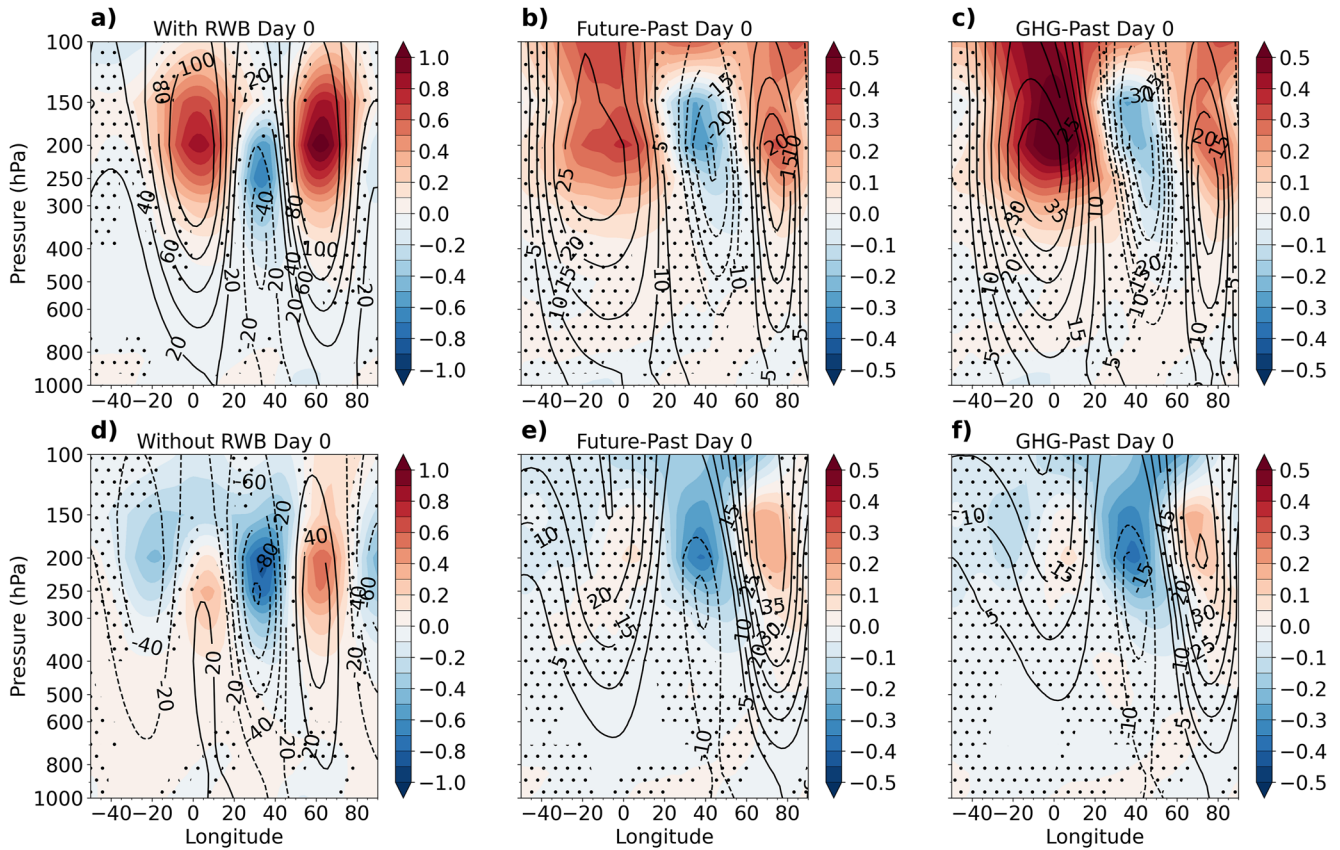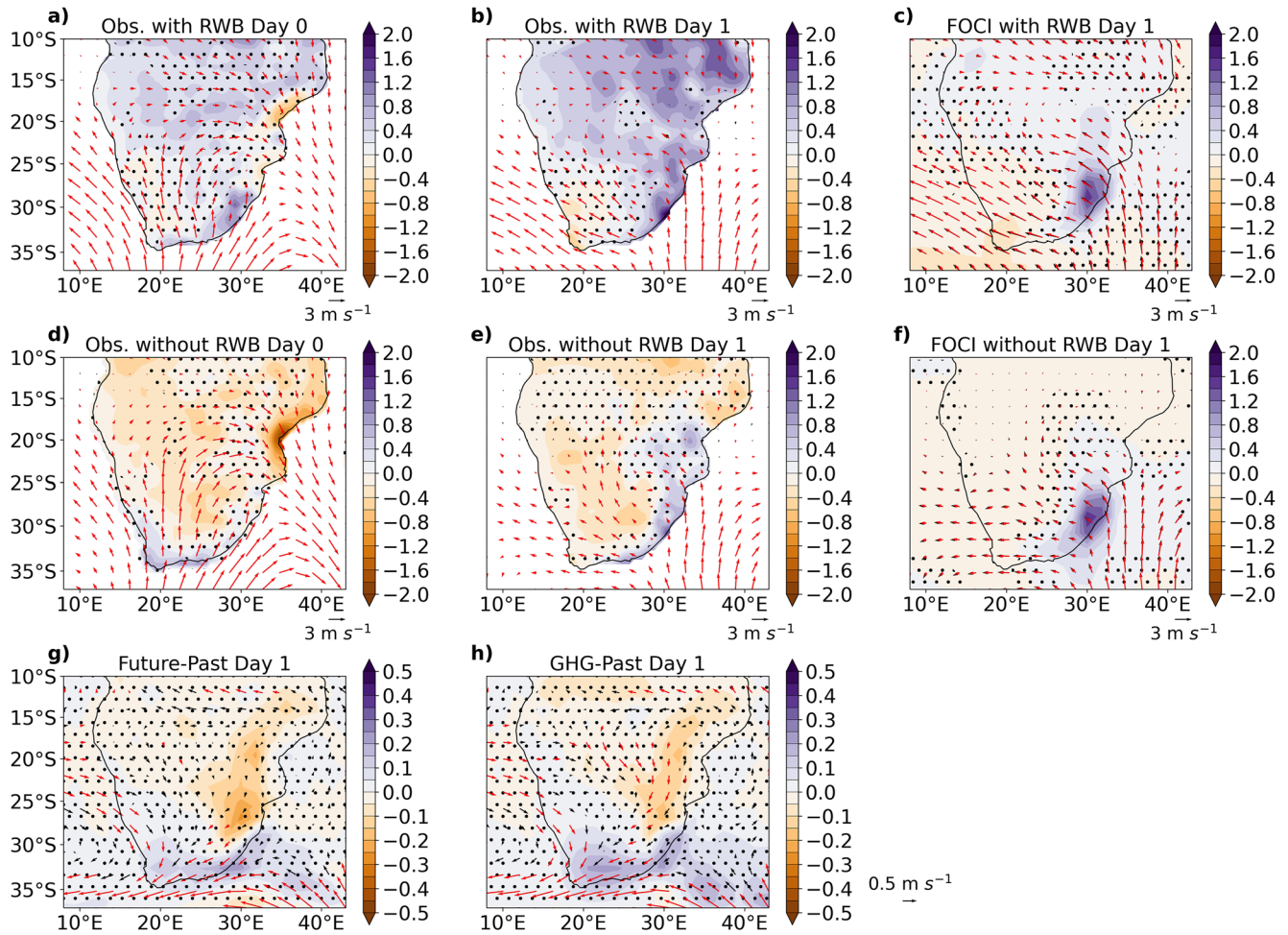
Figure 3. Composites of ridging highs (RHs) at day 0 with (a) and without (d) Rossby wave breaking (RWB) for the period 1980–2009. Anomalies of PV (PVU) and of geopotential height (m) at 45°S are depicted by the color shading and by the contours, respectively. Total (b, e) and greenhouse gase (GHG)-induced (c, f) change, between 2070–2099 and 1980–2009 at 50°S, in the anomalies associated with RHs with (b, c) and without (e, f) RWB. The stippling masks anomalies that are not significant at the 95% confidence interval. Only significant geopotential height anomalies are plotted.

confined south of the continent and negative anomalies cover most of southern Africa. This has important consequences for the flow and precipitation over the region, as discussed below.

MSLP anomalies seem to be well connected to PV anomalies aloft (contours in Figure 2) for RHs with RWB, but not as much for ridging high without RWB. Strong positive PV anomalies occur above the positive MSLP anomalies in Figures 2a and 2c, while weaker negative PV anomalies are found south of 40°S in the region of the negative MSLP anomalies. The dominant PV anomalies for the case without RWB are instead negative. There are no positive PV anomalies accompanying the positive MSLP anomalies between 0° and 40°E, suggesting that there is no clear connection between the ridging and the PV anomalies above.

To get a better understanding of the vertical coupling between PV and MSLP anomalies, Figure 3 shows the vertical profile of PV and geopotential height anomalies for the composites with and without RWB. The vertical profiles of composites using ERA5 are shown in Figure S3 in Supporting Information S1 and are in good agreement with the model composites, except for small differences in magnitude. The succession of positive, negative and again positive PV anomalies seen in Figure 3a clearly reveals the occurrence of RWB. These anomalies maximize around 200 hPa and extended between 400 and 100 hPa, inducing geopotential height anomalies of the same sign, in accordance with the PV invertibility principle (Hoskins et al., 1985). The geopotential height anomalies extend to the surface where they result in ridging. It thus appears that RWB close to the tropopause can induce RHs over South Africa. As discussed above, RHs also occur in the absence of RWB. While PV anomalies can also be seen in this case (Figure 3d), indicating that the PV contours are undulating as Rossby waves propagate without breaking, the positive anomalies between 0° and 30°E, where the ridging occurs, are much weaker. The positive geopotential height anomalies found at these longitudes seem to have their origin at lower levels, unlike in the case with RWB, and the ridging appears to be less influenced by the PV anomalies aloft.

Figure 4. Composites of ridging highs (RHs) with (a–c) and without (d–f) Rossby wave breaking (RWB) from observations (a, b, d, e) and from FOCI (c, f) at day 0 (a, d) and day 1 (b, c, e, f) for the period 1980–2009. Anomalies of precipitation (mm day^{-1}) and of 850 hPa winds (m s^{-1}) are depicted by the color shading and by the vectors, respectively. Total (g) and greenhouse gase (GHG)-induced (h) change, between 2070–2099 and 1980–2009, in the day 1 anomalies associated with RHs with RWB. The stippling masks anomalies that are not significant at the 95% confidence interval. The red vectors depict significant wind anomalies.

We demonstrated that RHs occurring with and without RWB are characterized by different patterns of MSLP anomalies, which naturally affect the flow of moist air from the warm Indian Ocean toward South Africa. Next, we explore the influence of these differences on precipitation.

3.2. Implications for Precipitation

Figure 4 shows annual composites of precipitation and 850 hPa winds for RHs with and without RWB, while seasonal composites are shown in the Supporting Information S1. As there is less agreement between model and observations regarding the precipitation anomalies compared to other fields, we discuss both model and observations in the following.

RHs with RWB are related to precipitation in both the all-year rainfall region and in the summer rainfall region in observations. At day 0 southerly onshore wind anomalies associated with the ridging bring moisture along the south coast resulting in positive precipitation anomalies (Figure 4a). As the ridging matures, positive MSLP anomalies are found south of the continent (Figure 2c) and the southerly wind anomalies are confined to the eastern part of South Africa (Figure 4b), while to the west southeasterly wind anomalies are present. Consequently, positive precipitation anomalies occur in the east, extending into Mozambique, while negative anomalies occur along the western coast. The model shows similar results, but overestimates the extent of the negative anomalies and underestimates the extent of the positive anomalies (Figure 4c). The southerly wind anomalies induced

by RHs with RWB are consistent with the ridging-associated circulation reported during extreme precipitation events by Crimp and Mason (1999) and Blamey and Reason (2009) that advects moisture to the eastern coast. RHs with RWB contribute most to precipitation over South Africa in autumn (Figures S4 and S5 in Supporting Information S1), as this is the season when COLs, often accompanying RHs and providing the air lifting mechanism, are most frequent (Singleton & Reason, 2007). Important contributions are additionally evident in spring and summer along the eastern coast and during winter along the south and southwest coasts.

RHs without RWB lead to more precipitation over the southwestern coast at day 0 (Figure 4d) compared to ridging high with RWB, exclusively in winter (Figure S6 in Supporting Information S1). Elsewhere they contribute significantly less precipitation over South Africa in the annual mean. Negative precipitation anomalies cover the inland from spring to autumn (Figures S6 and S7 in Supporting Information S1). This is the consequence of the positive MSLP anomalies extending over the continent at day 1 (Figure 2d) and resulting in weaker onshore wind anomalies that transport less moisture on land (Figure 4e). The drier conditions that occur in the absence of RWB are further explained by the fact that RWB promotes precipitation by leading to strong uplift to the east of its trough. Along the eastern coast, at day 1, positive anomalies occur, though weaker than in the case with RWB in the annual mean. On a seasonal basis, in this region RHs without RWB lead to more precipitation during summer, but RHs with RWB lead to more precipitation in autumn (Figures S5, S7 in Supporting Information S1). The strong precipitation contribution of RHs without RWB in summer is smoothed in the annual mean, particularly since considerably less events occur in this season than in winter and spring (Figure S1 in Supporting Information S1).

Despite simulating similar wind anomalies as found in the reanalysis, FOCI overestimates the amount of precipitation associated with RHs without RWB (Figure 4f). Climate models are known to overestimate precipitation in the region, particularly over the eastern part of South Africa (Almazroui et al., 2020; Dedekind et al., 2016; Engelbrecht et al., 2009; Jury, 2012). The atmospheric resolution in FOCI, like in other climate models, is too coarse to resolve important processes for precipitation, such as cloud processes. Convection has to be parameterized, but this leads to a misrepresentation of the diurnal cycle in convective rainfall (Nikulin et al., 2012). The diurnal cycle of convection and the intensity of precipitation extremes are improved in convection-resolving models (Ban et al., 2014). Therefore, the precipitation biases in FOCI are attributed to the convection parameterization, with the representation of the surface latent heat flux in the region possibly also playing a role (Jury, 2012).

3.3. Impact of Climate Change

We examine the future changes in RHs and their associated precipitation over the twenty-first century by taking the difference between annual composites for the FUTURE and the PAST ensembles, separately for RHs with and without RWB. As the westerly jet shifts poleward under climate change (Ivanciu et al., 2022; McLandress et al., 2011), so does RWB on the equatorward flank of the jet (Barnes & Hartmann, 2012). The pattern of negative PV change centered at 35°S and positive PV change centered at 50°S shown in Figure 2e illustrate the shift in RWB clearly. The positive PV anomalies induce positive geopotential height anomalies that reach the surface (Figure 3b), such that the positive MSLP anomalies associated with RHs in the future extend farther south (Figure 2e).

The negative PV anomaly accompanying RHs without RWB also moves poleward in the future causing negative MSLP anomalies (Figures 2f and 3e), but there is no change in the positive anomalies south of Africa, associated with the ridging. RWB thus mediates the impact of climate change on RHs and RHs that occur without RWB are less impacted in the future.

The differences between composites for the GHG and PAST ensemble (Figures 2g and 2h and Figures 3c and 3f) reveal that the increase in GHGs is responsible for the majority of the changes described above, while the differences between OZONE and PAST (not shown) are mostly not significant. Ivanciu et al. (2022) showed that changes in the westerly jet due to ozone recovery are considerably weaker than changes due to increased GHGs following SSP585, likely explaining why ozone recovery does not affect RHs.

Twenty-first century model simulations predict a decrease in precipitation over the entire southern Africa (Dosio et al., 2019; Rojas et al., 2019). The changes in RHs with RWB discussed above contribute to the drying in the eastern part of the subcontinent (Figure 4g). In contrast, along the south coast they lead to an increase in

precipitation, therefore weakening the total drying trend. The GHG-induced precipitation changes associated with RHs (Figure 4h) match the changes shown in Figure 4g very well, demonstrating that the increase in GHGs is driving these changes. The simulated precipitation changes come with the caveat that there are differences between the observed and modeled precipitation associated with RHs, as discussed above.

4. Conclusions

This study separated RHs over South Africa for the first time based on whether they occur together with RWB at tropopause levels or not in a state-of-the-art global coupled climate model and in the ERA5 reanalysis. In 43% (44%) of the cases RWB occurred together with the RHs in the model (reanalysis), a consistent result.

Positive PV anomalies associated with RWB induce positive geopotential height anomalies that reach to the surface and cause the South Atlantic Anticyclone to ridge. RHs can also occur in the absence of RWB. The patterns of MSLP anomalies related to RHs with and without RWB differ. Stronger southerly and southeasterly wind anomalies occur in the presence of RWB. Previous studies showed that such wind anomalies advect moisture-laden air from above the warm Agulhas Current into South Africa (Blamey & Reason, 2009; Crimp & Mason, 1999; Rapolaki et al., 2020). Therefore, RHs with RWB lead to increased precipitation along the southern coast at day 0 and in the eastern part of the county at days 0 and 1. The observational-based composites demonstrated that RHs that occur accompanied by RWB bring more precipitation over southern Africa in the annual mean than RHs without RWB. Although there is good agreement between the model and ERA5 with respect to most fields, larger differences arise with respect to precipitation, with the model underestimating (overestimating) the extent of the positive (negative) anomalies associated with RHs with RWB and exhibiting a positive precipitation bias for RHs without RWB. Climate models have known difficulties in correctly simulating the precipitation in the region, attributed to their convective parameterization schemes that do not represent the diurnal cycle realistically (Nikulin et al., 2012).

The twenty-first century changes in RHs were additionally investigated for the first time. RWB on the equatorward side of the westerly jet shifts poleward with the jet in the future, mediating the effect of climate change on RHs. Accordingly, the positive MSLP anomalies associated with the ridging extend farther south. RHs that occur without RWB experience little change. The model predicts that RHs with RWB will bring more precipitation over the south coast and less precipitation in the eastern part of southern Africa in the future. The increase in GHGs according to the SSP585 scenario is the main driver of the future changes, while ozone recovery does not affect RHs, likely because its effect on the westerly jet is considerably weaker (Ivanciu et al., 2022).

Data Availability Statement

The model output used in this study is available at https://doi.org/10.5281/zenodo.6523956 (Ivanciu, 2022). The ERA5 hourly data on pressure levels from 1979 to present (Hersbach et al., 2018) is publicly available from the Copernicus Climate Change Service (C3S) Climate Data Store (CDS) at https://doi.org/10.24381/cds.bd0915c6 (accessed on 16.05.2020). The CPC Global Unified Gauge-Based Analysis of Daily Precipitation data is provided by the NOAA PSL, Boulder, Colorado, USA, from their Web site at https://psl.noaa.gov/data/gridded/data.cpc.globalprecip.html (accessed on 16.05.2022).

References

Almazroui, M., Saeed, F., Saeed, S., Nazrul Islam, M., Ismail, M., Klutse, N. A. B., & Siddiqui, M. H. (2020). Projected change in temperature and precipitation over Africa from CMIP6. *Earth Systems and Environment*, 4(3), 455–475. https://doi.org/10.1007/s41748-020-00161-x

Ban, N., Schmidli, J., & Schär, C. (2014). Evaluation of the convection-resolving regional climate modeling approach in decade-long simulations. *Journal of Geophysical Research: Atmospheres*, 119(13), 7889–7907. https://doi.org/10.1002/2014JD021478

Barnes, E. A., & Hartmann, D. L. (2012). Detection of Rossby wave breaking and its response to shifts of the midlatitude jet with climate change. *Journal of Geophysical Research*, 117(D9). https://doi.org/10.1029/2012JD017469

Blamey, R. C., & Reason, C. J. C. (2009). Numerical simulation of a mesoscale convective system over the East Coast of South Africa. *Tellus A: Dynamic Meteorology and Oceanography*, 61(1), 17–34. https://doi.org/10.1111/j.1600-0870.2007.00366.x

Blamey, R. C., & Reason, C. J. C. (2012). Mesoscale convective complexes over southern Africa. *Journal of Climate*, 25(2), 753–766. https://doi.org/10.1175/JCLI-D-10-05013.1

Chen, M., Shi, W., Xie, P., Silva, V. B. S., Kousky, V. E., Wayne Higgins, R., & Janowiak, J. E. (2008). Assessing objective techniques for gauge-based analyses of global daily precipitation. *Journal of Geophysical Research*, 113(D4), D04110. https://doi.org/10.1029/2007JD009132

Crimp, S. J., & Mason, S. J. (1999). The extreme precipitation event of 11 to 16 February 1996 over South Africa. *Meteorology and Atmospheric Physics*, 70(1–2), 29–42. https://doi.org/10.1007/s007030050023

Dedekind, Z., Engelbrecht, F. A., & van der Merwe, J. (2016). Model simulations of rainfall over southern Africa and its eastern escarpment. *Water SA*, *42*(1), 129–143. https://doi.org/10.4314/wsa.v42i1.13

Dosio, A., Jones, R. G., Jack, C., Lennard, C., Nikulin, G., & Hewitson, B. (2019). What can we know about future precipitation in Africa? Robustness, significance and added value of projections from a large ensemble of regional climate models. *Climate Dynamics*, *53*(9–10), 5833–5858. https://doi.org/10.1007/s00382-019-04900-3

Dyson, L. L. (2015). A heavy rainfall sounding climatology over Gauteng, South Africa, using self-organising maps. *Climate Dynamics*, *45*(11–12), 3051–3065. https://doi.org/10.1007/s00382-015-2523-3

Engelbrecht, C. J., Landman, W. A., Engelbrecht, F. A., & Malherbe, J. (2015). A synoptic decomposition of rainfall over the Cape south coast of South Africa. *Climate Dynamics*, *44*(9–10), 2589–2607. https://doi.org/10.1007/s00382-014-2230-5

Engelbrecht, F. A., McGregor, J. L., & Engelbrecht, C. J. (2009). Dynamics of the conformal-cubic atmospheric model projected climate-change signal over southern Africa. *International Journal of Climatology*, *29*(7), 1013–1033. https://doi.org/10.1002/joc.1742

Favre, A., Hewitson, B., Lennard, C., Cerezo-Mota, R., & Tadross, M. (2013). Cut-off Lows in the South Africa region and their contribution to precipitation. *Climate Dynamics*, *41*(9–10), 2331–2351. https://doi.org/10.1007/s00382-012-1579-6

Harrison, M. S. J. (1984). A generalized classification of South African summer rain-bearing synoptic systems. *Journal of Climatology*, *4*(5), 547–560. https://doi.org/10.1002/joc.3370040510

Hart, N. C. G., Reason, C. J. C., & Fauchereau, N. (2012). Building a tropical–extratropical cloud band metbot. *Monthly Weather Review*, *140*(12), 4005–4016. https://doi.org/10.1175/MWR-D-12-00127.1

Hart, N. C. G., Reason, C. J. C., & Fauchereau, N. (2013). Cloud bands over southern Africa: Seasonality, contribution to rainfall variability and modulation by the MJO. *Climate Dynamics*, *41*(5–6), 1199–1212. https://doi.org/10.1007/s00382-012-1589-4

Hersbach, H., Bell, B., Berrisford, P., Biavati, G., Horányi, A., Muñoz Sabater, J., et al. (2018). ERA5 hourly data on pressure levels from 1979 to present. Copernicus climate change Service (C3S) climate data Store (CDS). [dataset]. (Accessed on 16.05.2022). https://doi.org/10.24381/cds.bd0915c6

Hersbach, H., Bell, B., Berrisford, P., Hirahara, S., Horányi, A., Muñoz-Sabater, J., et al. (2020). The ERA5 global reanalysis. *Quarterly Journal of the Royal Meteorological Society*, *146*(730), 1999–2049. https://doi.org/10.1002/qj.3803

Hoskins, B. J., McIntyre, M. E., & Robertson, A. W. (1985). On the use and significance of isentropic potential vorticity maps. *Quarterly Journal of the Royal Meteorological Society*, *111*(470), 877–946. https://doi.org/10.1002/qj.49711147002

Ivanciu, I. (2022). FOCI model output used in the study by Ivanciu et al. - On the ridging of the South Atlantic Anticyclone over South Africa: The impact of Rossby wave breaking and of climate change [dataset]. Zenodo. https://doi.org/10.5281/zenodo.6523955

Ivanciu, I., Matthes, K., Biastoch, A., Wahl, S., & Harlaß, J. (2022). Twenty-first-century Southern Hemisphere impacts of ozone recovery and climate change from the stratosphere to the ocean. *Weather and Climate Dynamics*, *3*(1), 139–171. https://doi.org/10.5194/wcd-3-139-2022

Ivanciu, I., Matthes, K., Wahl, S., Harlaß, J., & Biastoch, A. (2021). Effects of prescribed CMIP6 ozone on simulating the Southern Hemisphere atmospheric circulation response to ozone depletion. *Atmospheric Chemistry and Physics*, *21*(8), 5777–5806. https://doi.org/10.5194/acp-21-5777-2021

Jury, M. R. (2012). An inter-comparison of model-simulated east–west climate gradients over South Africa. *Water SA*, *38*(4), 467–478. https://doi.org/10.4314/wsa.v38i4.1

Jury, M. R., & Goschen, W. S. (2020). Physical ocean-atmosphere variability over the shelf of South Africa from reanalysis products. *Continental Shelf Research*, *202*, 104135. https://doi.org/10.1016/j.csr.2020.104135

Kinnison, D. E., Brasseur, G. P., Walters, S., Garcia, R. R., Marsh, D. R., Sassi, F., et al. (2007). Sensitivity of chemical tracers to meteorological parameters in the MOZART-3 chemical transport model. *Journal of Geophysical Research*, *112*(D20), D20302. https://doi.org/10.1029/2006JD007879

Lee-Thorp, A. M., Rouault, M., & Lutjeharms, J. R. E. (1999). Moisture uptake in the boundary layer above the Agulhas Current: A case study. *Journal of Geophysical Research*, *104*(C1), 1423–1430. https://doi.org/10.1029/98JC02375

Matthes, K., Biastoch, A., Wahl, S., Harlaß, J., Martin, T., Brücher, T., et al. (2020). The Flexible Ocean and Climate Infrastructure version 1 (FOCI1): Mean state and variability. *Geoscientific Model Development*, *13*(6), 2533–2568. https://doi.org/10.5194/gmd-13-2533-2020

McIntyre, M. E., & Palmer, T. N. (1983). Breaking planetary waves in the stratosphere. *Nature*, *305*(5935), 593–600. https://doi.org/10.1038/305593a0

McLandress, C., Shepherd, T. G., Scinocca, J. F., Plummer, D. A., Sigmond, M., Jonsson, A. I., & Reader, M. C. (2011). Separating the dynamical effects of climate change and ozone depletion. Part II: Southern Hemisphere troposphere. *Journal of Climate*, *24*(6), 1850–1868. https://doi.org/10.1175/2010JCLI3958.1

Ndarana, T., Bopape, M.-J., Waugh, D., & Dyson, L. (2018). The influence of the lower stratosphere on ridging Atlantic Ocean Anticyclones over South Africa. *Journal of Climate*, *31*(15), 6175–6187. https://doi.org/10.1175/JCLI-D-17-0832.1

Ndarana, T., Mpati, S., Bopape, M.-J., Engelbrecht, F., & Chikoore, H. (2021). The flow and moisture fluxes associated with ridging South Atlantic Ocean Anticyclones during the subtropical southern African summer. *International Journal of Climatology*, *41*(S1), E1000–E1017. https://doi.org/10.1002/joc.6745

Ndarana, T., Rammopo, T. S., Reason, C. J., Bopape, M.-J., Engelbrecht, F., & Chikoore, H. (2022). Two types of ridging South Atlantic Ocean Anticyclones over South Africa and the associated dynamical processes. *Atmospheric Research*, *265*, 105897. https://doi.org/10.1016/j.atmosres.2021.105897

Ndarana, T., & Waugh, D. W. (2011). A climatology of Rossby wave breaking on the Southern Hemisphere tropopause. *Journal of the Atmospheric Sciences*, *68*(4), 798–811. https://doi.org/10.1175/2010JAS3460.1

Nikulin, G., Jones, C., Giorgi, F., Asrar, G., Büchner, M., Cerezo-Mota, R., et al. (2012). Precipitation climatology in an ensemble of CORDEX-Africa regional climate simulations. *Journal of Climate*, *25*(18), 6057–6078. https://doi.org/10.1175/JCLI-D-11-00375.1

Nkwinkwa Njouodo, A. S., Koseki, S., Keenlyside, N., & Rouault, M. (2018). Atmospheric signature of the Agulhas Current. *Geophysical Research Letters*, *45*(10), 5185–5193. https://doi.org/10.1029/2018GL077042

Nkwinkwa Njouodo, A. S., Rouault, M., Keenlyside, N., & Koseki, S. (2021). Impact of the Agulhas Current on southern Africa precipitation: A modelling study. *Journal of Climate*, 1–50. https://doi.org/10.1175/JCLI-D-20-0627.1

Rapolaki, R. S., Blamey, R. C., Hermes, J. C., & Reason, C. J. C. (2020). Moisture sources associated with heavy rainfall over the Limpopo River Basin, southern Africa. *Climate Dynamics*, *55*(5–6), 1473–1487. https://doi.org/10.1007/s00382-020-05336-w

Roffe, S., Fitchett, J., & Curtis, C. (2019). Classifying and mapping rainfall seasonality in South Africa: A review. *South African Geographical Journal*, *101*(2), 158–174. https://doi.org/10.1080/03736245.2019.1573151

Rojas, M., Lambert, F., Ramirez-Villegas, J., & Challinor, A. J. (2019). Emergence of robust precipitation changes across crop production areas in the 21st century. *Proceedings of the National Academy of Sciences*, *116*(14), 6673–6678. https://doi.org/10.1073/pnas.1811463116

Rouault, M., Lee-Thorp, A. M., & Lutjeharms, J. R. E. (2000). The atmospheric boundary layer above the Agulhas Current during Alongcurrent winds. *Journal of Physical Oceanography*, *30*(1), 40–50. https://doi.org/10.1175/1520-0485(2000)030<0040:TABLAT>2.0.CO;2

Rouault, M., Reason, C. J. C., Lutjeharms, J. R. E., & Beljaars, A. C. M. (2003). Underestimation of latent and sensible heat fluxes above the Agulhas Current in NCEP and ECMWF analyses. *Journal of Climate*, *16*(4), 776–782. https://doi.org/10.1175/1520-0442(2003)016<0776:UOLASH>2.0.CO;2

Rouault, M., White, S. A., Reason, C. J. C., Lutjeharms, J. R. E., & Jobard, I. (2002). Ocean–atmosphere interaction in the Agulhas Current region and a South African extreme weather event. *Weather and Forecasting*, *17*(4), 655–669. https://doi.org/10.1175/1520-0434(2002)017<0655:oaiita>2.0.co;2

Schwarzkopf, F. U., Biastoch, A., Böning, C. W., Chanut, J., Durgadoo, J. V., Getzlaff, K., et al. (2019). The INALT family – A set of high-resolution nests for the Agulhas Current System within global NEMO ocean/sea-ice configurations. *Geoscientific Model Development*, *12*(7), 3329–3355. https://doi.org/10.5194/gmd-12-3329-2019

Singleton, A. T., & Reason, C. J. C. (2006). Numerical simulations of a severe rainfall event over the Eastern Cape coast of South Africa: Sensitivity to sea surface temperature and topography. *Tellus A: Dynamic Meteorology and Oceanography*, *58*(3), 335–367. https://doi.org/10.1111/j.1600-0870.2006.00180.x

Singleton, A. T., & Reason, C. J. C. (2007). Variability in the characteristics of cut-off low pressure systems over subtropical southern Africa. *International Journal of Climatology*, *27*(3), 295–310. https://doi.org/10.1002/joc.1399

Tyson, P. D., & Preston-Whyte, R. A. (2000). *Weather and climate of southern Africa*. Oxford University Press.

Wirth, V., Riemer, M., Chang, E. K. M., & Martius, O. (2018). Rossby wave packets on the midlatitude waveguide—A review. *Monthly Weather Review*, *146*(7), 1965–2001. https://doi.org/10.1175/MWR-D-16-0483.1

References From the Supporting Information

Edouard, S., Vautard, R., & Brunet, G. (1997). On the maintenance of potential vorticity in isentropic coordinates. *Quarterly Journal of the Royal Meteorological Society*, *123*(543), 2069–2094. https://doi.org/10.1002/qj.49712354314